Journal of Molecular Structure 1080 (2015) 145–152

Contents lists available at ScienceDirect

Journal of Molecular Structure

journal homepage: www.elsevier.com/locate/molstruc

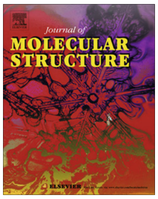

Quantum mechanical and experimental analyses of TNT metabolite 2-hydroxylamino-4,6-dinitrotoluene

Thomas Junk [a], Yuemin Liu [a], Zhong Li [b], Richard Perkins [a], Yucheng Liu [c,]*

[a] *Department of Chemistry, University of Louisiana at Lafayette, Lafayette, LA 70504, United States*
[b] *Department of Chemistry, University of Louisiana at Monroe, Monroe, LA 71209, United States*
[c] *Department of Mechanical Engineering, Mississippi State University, MS 39759, United States*

HIGHLIGHTS

- Quantum mechanical MP2/aug-cc-pVDZ simulations of 2-HADNT for geometry optimizations and conformational energy profile.
- Single point MP2/aug-cc-pVDZ calculations of chemical properties.
- Energy minimum structures are found to be very close to the crystal structure.
- The 4-nitro group exhibits co-planarity with the phenyl ring in both crystal and energy minimization structures.
- This work demonstrates considerable discrepancies of some results between MP2 and B3LYP methods.

ARTICLE INFO

Article history:
Received 22 July 2014
Received in revised form 21 September 2014
Accepted 21 September 2014
Available online 5 October 2014

Keywords:
2-HADNT
MP2
HUMO–LUMO separation
Conjugation
Dipole

ABSTRACT

In this study, a combined quantum mechanical and experimental analyses were performed to investigate crystal structure of the immediate degradation product of TNT, 2-hydroxylamino-4,6-dinitrotoluene (2-HADNT) and to reveal its important chemical properties. Leakage of 2-HADNT has caused serious environmental pollution and therefore raises widespread concerns. In the quantum mechanical analysis, the B3LYP/6-311+G**, B3LYP/aug-c-pVDZ, M06HF/aug-cc-pVDZ, and MP2/aug-cc-pVDZ methods were employed for geometrical optimization and single point calculations of chemical properties of the compound. Such properties include highest unoccupied molecular orbitals (HOMO) – lowest occupied molecular orbitals (LUMO) separation, dipole moment, atomization energy, and vibrational frequencies. Experimental analysis and validation showed that the energy minimized structures acquired from the quantum mechanical analysis were very similar to those obtained by X-ray crystallography. The 6-NO_2 groups twist out of plane with respect to the benzene ring in both the crystallographic and energy minimized structures. The 4-NO_2 group exhibits co-planarity with the phenyl ring in both the crystallographic and energy minimized structures as well. Unlike TNT, however, the energy barrier to orthogonal conformation is only 3.8 kcal/mol. In addition, considerable discrepancies between results obtained from the MP2 and B3LYP methods were observed, which suggest that it has to be very careful when applying B3LYP method to study such class of compounds. Through this study, a more accurate description of the chemical properties of dispersion-dominated aromatic systems was acquired. The chemical properties found from this study can help researchers to better understand the compound of 2-HADNT and to develop effective management plans for such compound so as to minimize its impact on the environment.

Introduction

The explosive 2,4,6-trinitrotoluene (TNT) has been widely used for military and commercial purposes for centuries [1–3]. However, the extensive application of TNT resulted in significant environmental contaminations through carcinogenic TNT and its metabolites, and environmental remediation is therefore highly wanted [4,5]. It is well known that TNT mineralizes slowly, mostly follows reductive pathways and gives rise to toxic intermediates including 2-hydroxylamino-4,6-dinitrotoluene [6–11]. In order to effectively implement environmental remediation, analytical and toxicological evaluations of contaminated sites are required and therefore a thorough knowledge of the properties of the reduction

---

* Corresponding author. Tel.: +1 337 382 5822; fax: +1 337 482 1129.
E-mail address: yxl5763@louisiana.edu (Y. Liu).

http://dx.doi.org/10.1016/j.molstruc.2014.09.058
0022-2860/

products such as hydroxylamino-, amino-, azo-, and azoxytoluenes is highly wanted. It was found that initial products of TNT reductive degradation are 2-hydroxylamino-4,6-dinitrotoluene (2-HADNT) and its isomer 4-hydroxylamino-2, 6-dinitrotoluene (4-HADNT), as shown in Fig. 1 [11–13]. Homma-Takeda et al. found that 4-HADNT damages DNA, prompts the generation of 8-oxodG, and causes cleavage of DNA at sites with consecutive guanines [14]. It was also agreed that an understanding of the chemical properties of these initial TNT reduction products may provide insight into their reductive pathways and environmental fates [15]. Unfortunately, as pointed out by Junk, Catallo, and Maeda, limited access to various TNT degradation products remains a significant barrier in collecting experimental data from those materials and performing experimental analysis [11,13]. Quantum mechanical simulation can be an advanced and alternative method to evaluate their thermo-chemical properties. However, such method has to be validated by comparing the quantum mechanical simulation results with the experimental data.

In this paper, two Density Functional Theory (DFT) methods and high level second order Møller–Plesset perturbation theory (MP2) method were applied to calculate the chemical properties of 2-HADNT and the simulation results were compared with the experimental data obtained from X-ray crystallography. Important chemical properties include the LUMO–HOMO separation [10,16], dipole moment, and atomization energy. Especially, in this study, the structural parameters of 2-HADNT were compared with the published structural parameters for TNT [17–20] and their differences were highlighted.

Regarding the employed research tools, the DFT methods have been widely used in theoretical simulations of TNT and its derivatives [10,16,21–31], whereas the application of MP2 methods are relatively limited due to its high computational cost [24,29,31]. However, the most popular DFT method B3LYP [32–35] was found being inaccurate in simulating dispersion-dominated non-covalent interactions [36]. In fact, mPWB1K/TZVP was found to be the most accurate DFT for computing the reduction potential of nitrobenzenes [37]. On the other hand, the vibrational frequencies calculated using B3LYP/6-311+G** were found to best agree with those determined by infrared spectrum (IR) [30]. Based on these reasons, this study targeted the quantum mechanical simulation of 2-HADNT using the B3LYP and MP2/aug-cc-pVDZ methods. The simulation results were then compared with the data obtained from X-ray crystallography as well as the published results for TNT. A more accurate description of the chemical properties of dispersion-dominated aromatic systems was acquired through this study.

Research approach

Computational method

In the mechanical simulation, computer models were generated for molecular structure, which was the optimized structure at MP2 level based on the compound's crystal structure (the molecular structure can be seen from Fig. 1). Initial coordinates derived from the crystal structure of 2-HADNT were optimized with MP2/aug-cc-pVDZ using Gaussian-09 [38]. Based on the computer models, important chemical properties such as LUMO–HOMO gap, dipole moment and atomic energy were then calculated using the B3LYP, M06HF, and MP2 methods. The calculated conformational energy profile of 2-HADNT was then compared with a published conformational energy profile of TNT (entry ZZZMUC01), obtained from the Cambridge Crystallographic Data Centre [17]. The aug-cc-pVDZ basis sets were used throughout all single point calculations, and the results were compared with those obtained using the basis set 6-311+G**. In order to compare with the experimental data, solvation effects need to be considered [39,40]. In this work, solvation effects were considered for single point calculations only and solvation corrections were implemented using the polarizable continuum model (SMD) [41] with a dielectric constant of 4.7 for an aqueous solution [42]. Minimized structures were confirmed by an absence of negative frequencies in vibrational frequency calculations. All the computational simulations and calculations were performed on a quad-core cluster canpe01 and dual-core canfire04 at the Center for Advanced Computer Studies (CACS) at the University of Louisiana at Lafayette with support of high performance computational resources provided by the Louisiana Optical Network Initiative (LONI).

Experimental method

In experimental analysis 2-HADNT was synthesized following a procedure presented by Junk and Catallo [11]. In that procedure, a Fourier transformation infrared (FTIR) sample of 2-HADNT was first mixed with KBr and was compressed to a thin layer for IR analysis. In our study, FTIR spectra were determined using a JASCO FI/IR-480 spectrometer with an attached continuum micro-

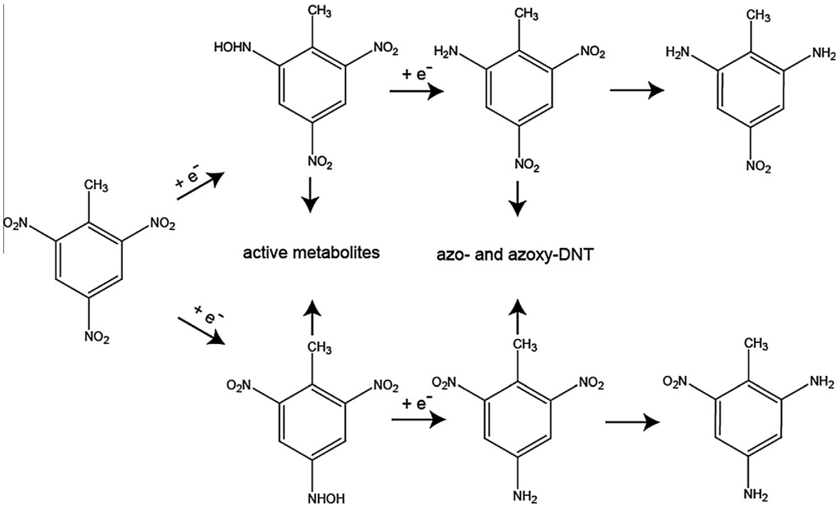

Fig. 1. Reductive degradation pathway of TNT.

scope. Raman spectra were measured at incident wavelength of 514 nm using SPEX 1403 0.85 m Double monochromator Spectrometer. The obtained experimental results were then compared with the simulation results to validate the employed research approaches.

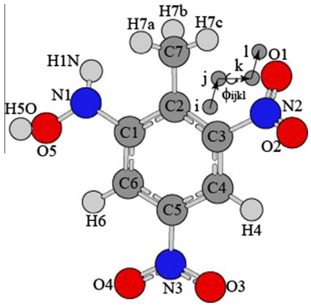

Fig. 2. Schematic structure of 2-HADNT displaying numbering scheme.

Results and preliminary discussion

In post-processing, the optimized torsion angles for 2-HADNT calculated from the mechanical simulation were compared with the angles measured from experiments (crystallography), as well as with the published angle values for TNT. The comparison results are listed in Table 1 and the numbering scheme of 2-HADNT is shown in Fig. 2.

From above table, it can be found that the O2–N2–C3–C2 dihedral angle associated with 6-NO_2 is most affected by different chemical models used (MP2 vs. B3LYP). This may be because of differences in the treatment of steric methyl-nitro interactions (Fig. 3d). The respective optimized torsion angles are 46.5° for MP2/aug-cc-pVDZ and 38.5° for B3LYP/aug-cc-pVDZ.

Comparing to the 2-nitro group in TNT, the –NHOH moiety in 2-HADNT results in reduced steric interaction with the methyl moiety and strengthened resonance conjugation with the aromatic ring due to its electron donating effect. As depicted in Fig. 3a, the most stable conformation differs from the least stable by about 7 kcal/mol. The O5–N1–C1–C6 dihedral angles were found to be 10.0°, 12.6°, 14.7°, and 15.7° respectively for the crystal, B3LYP/6-311+G**, B3LYP/aug-cc-pVDZ, and MP2/aug-cc-pVDZ structures. The 4-nitro group adopts co-planarity with phenyl ring due to conjugation. Specifically, the difference between the most stable co-planar conformation and the least stable one was found about 5.6 kcal/mol (Fig. 3b). Torsional O4–N3–C5–C6 angles indicating near-coplanarity of the 4-nitro group in 2-HADNT were 2.8° as measured from the crystal, and were calculated as 3.1° (B3LYP/6-311+G**), 2.1° (B3LYP/aug-cc-pVDZ), and 2.7° (MP2/aug-cc-pVDZ) according to different chemical models.

Relationship between the O2–N2–C3–C2 dihedral angle of 6-NO_2 and conformation dependent energy is displayed in Fig. 3c. 2-HADNT accommodates steric repulsion between methyl and nitro while retaining limited conjugation of nitro with the aromatic ring. This balance between the steric clash/repulsion of oxygen of 6-nitro with methyl group and p-π conjugation cross 6-nitro-phenyl ring is reflected through a relatively flat energy profile with amplitude of 2.0 kcal/mol as shown in that figure. The O2–N2–C3–C2 torsion angle of 54.3° measured from the crystalline 2-HADNT is very close to those angles of the 6-nitro groups of conformation A for monoclinic and orthorhombic TNT, which are 60°, −51.2°, and −57.5°, respectively [17–20,30]. The O2–N2–C3–C2 torsion angle was also calculated as 38.5° from B3LYP/6-311+G**, 37.8° from B3LYP/aug-cc-pVDZ, and 41.1° from B3LYP/1-311+G** for TNT [30]. Those values are close to each other, suggesting that neither crystal packing nor the replacement of 2-NO_2 by 2-NHOH significantly affects molecular geometry.

To evaluate the electron donating effect of 2-NHOH, potential energy surface scans were explored for the rotation of 4-NO_2 for both 2-HADNT and TNT using B3LYP (Fig. 4). The resulting potential energy landscape shows that the replacement of 2-NO_2 with 2-NHOH only led to minor changes on the potential energy. For both 2-HADNT and TNT, the co-planar conjugated configurations refer to minimum potential energy, and perpendicular un-conjugated conformations possess the highest energy among all possible conformations. The difference between the relative perpendicular conformational energy of 2-HADNT and that of TNT is about 0.2 kcal/mol, which confirms that the switch from a 2-NO_2 moiety of TNT to a 2-NHOH moiety of 2-HADNT has little influence on the conformational energy.

Table 1
Selected torsion angles for the 4-NO_2, 6-NO_2, and methyl groups of the crystal and calculated structures of 2-HADNT. Crystallographic parameters for TNT [17] are tabulated for comparison.

Dihedral	Crystal	B3LYP/6-311+G**	B3LYP/aug-cc-pVDZ	MP2/aug-cc-pVDZ
2-HADNT (°)				
2-NHOH (O5–N1–C1–C2)	10.0	12.6	14.7	15.7
4-NO_2 (O4–N3–C5–C6)	2.8	3.1	2.1	2.7
6-NO_2 (O2–N2–C3–C2)	54.3	38.5	37.8	46.5
1-CH_3 (C1–C2–C7–H7c)	17.5	18.5	18.1	19.2
Dihedral	Crystal [17]	B3LYP/6-311+G**	B3LYP/aug-cc-pVDZ	MP2/aug-cc-pVDZ
TNT (°)				
2-NO_2	43.0	40.1	41.0	50.3
4-NO_2	32.0	0.0	0.0	0.2
6-NO_2	60.0	40.1	40.1	50.3
1-CH_3	39.6	27.4	27.0	28.3

Dihedral	Crystal [30]				B3LYP/6-31G* [30]		B3LYP/6-311+G** [30]	
	Monoclinic		Orthorhombic					
Conformation	A	B	A	B	A	B	A	B
TNT (°)								
2-NO_2	47.2	59.5	42.1	53.1	33.4	31.8	41.1	41.0
4-NO_2	22.0	−32.2	35.3	−23.7	0.1	1.1	0.2	0.8
6-NO_2	−51.2	−40.9	−57.5	−46.4	−33.5	45.4	−41.1	52.2
1-CH_3	97.6	86.4	117.7	76.7	91.8	−14.2	91.8	−16.1

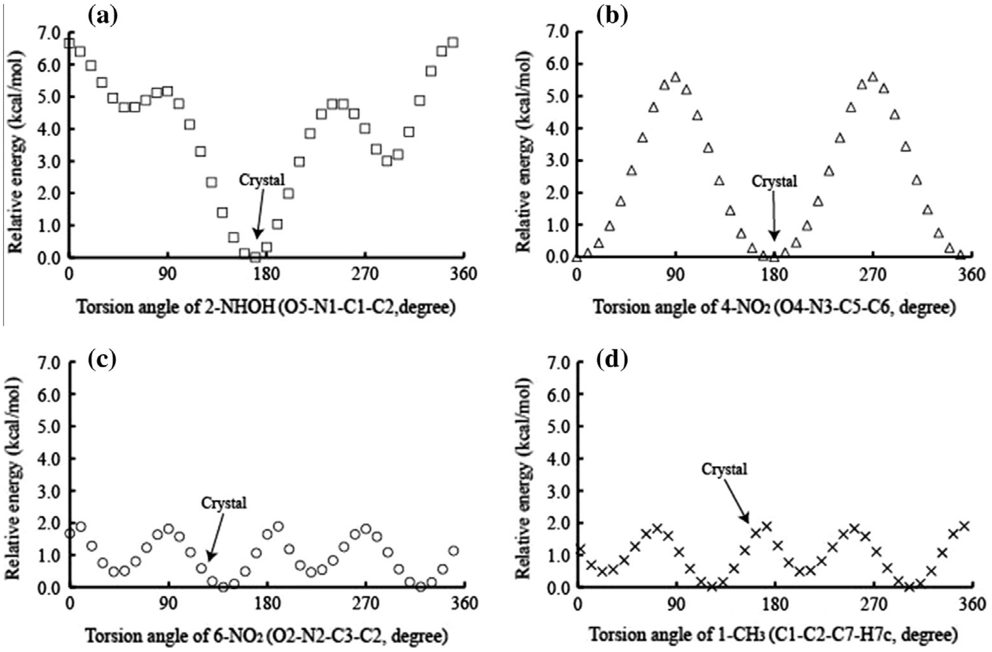

Fig. 3. Potential energy surface scans of 2-HADNT along the coordinates corresponding to rotations of 2-NHOH, 4-NO_2, and, 6-NO_2 with respect to the planar phenyl ring.

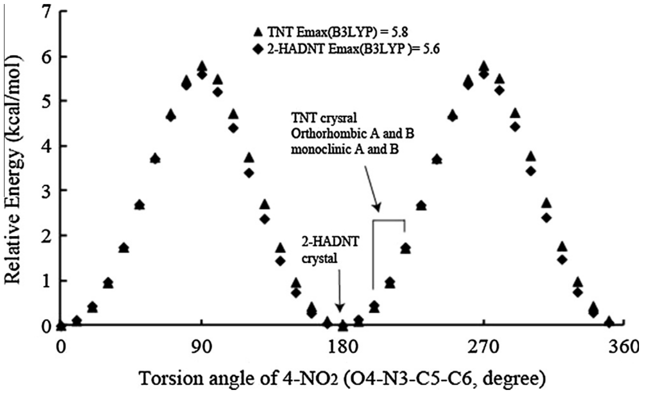

Fig. 4. Potential energy profile for the 4-nitro group, using B3LYP/aug-cc-pVDZ.

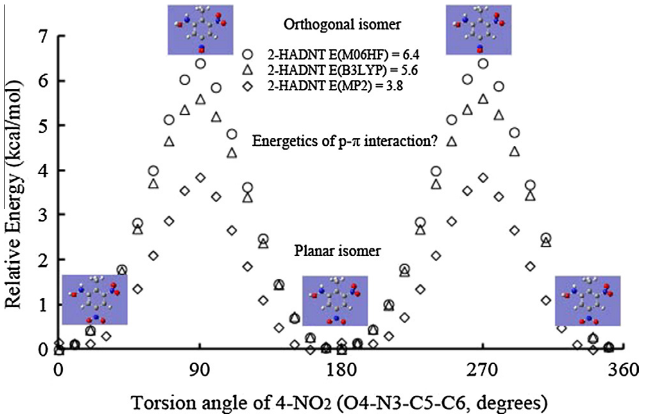

Fig. 5. Rotation energy profiles for 4-NO_2 in 2-HADNT obtained from M06HF/Aug-cc-pVDZ, B3LYP/aug-cc-pVDZ, and MP2/aug-cc-pVDZ methods.

The 4-nitro group does not experience intra-molecular interactions with neighboring moieties. Therefore it can be used to probe the effect of π-conjugation between 4-NO_2 and the phenyl ring, as can be seen from the different chemistry models. The energy difference between the coplanar and orthogonal conformations is known as the p-π conjugation stabilization energy (Fig. 5). From the conformational energy profiles, stabilization energy of 3.8 kcal/mol, 6.4 kcal/mol, and 6.5 kcal/mol were obtained using MP2, M06HF and B3LYP methods, respectively. Those results implied that only small amounts of energy expenses are incurred as the 4-NO_2 group deviates from the co-planarity. The conformational energy profiles were obtained by calculating the conformational energy with respect to different angles (from 0° to 360° with an increment of 5°) between the NO_2 plane and the phenyl ring plane. It should be noted, however, that significant discrepancies do exist between MP2 and DFT method. As it is well known that the MP2 method is a more accurate method than the DFT method, such discrepancies suggest that the DFT results should be further verified using *ab initio* calculations.

Chemical properties and method dependence

Table 2 lists the LUMO–HOMO energy separations, atomization energy, and dipole moments calculated based on the optimized structures of TNT, 2-HADNT, 4-HADNT, 2-amino-4,6-dinitrotoluene (2-ADNT), and 4-ADNT. Frontier orbital is displayed in Fig. 6. Additionally, LUMO–HOMO gaps and dipole moments were also calculated using B3LYP/6-311+G** and B3LYP/aug-cc-pVDZ for 2-HADNT for the purpose of method dependence evaluation (Table 3). Previously, the HOMO-LUMO gap of polycyclic aromatic hydrocarbons had served as a reasonable parameter for evaluating their kinetic stabilities [43–46]. Large HOMO–LUMO energy separations refer to high kinetic stability since they pose high energy barriers to add additional electrons to a relatively high-lying LUMO and to seize existing electrons from a relatively low-lying HOMO in transition states and intermediates. 2-HADNT has a LUMO–HOMO gap of 0.3710 eV, which is higher than that of 2-ADNT (0.3577 eV) but lower than that of TNT (0.4131 eV). Thus, kinetic stability of 2-HADNT should be lower than that of TNT but higher than that

Table 2
Chemical properties of TNT and its four degradation products calculated using MP2 methods (MO means molecular orbital).

Structure	LUMO (eV) (MO)	HOMO (eV) (MO)	LUMO–HOMO gap (eV)	Atomization energy (kcal/mol)	Dipole (Debye)
TNT	−0.0091(59)	−0.4222(58)	0.4131	−552471.2	1.27
2-HADNT	0.0136(56)	−0.3574(55)	0.3710	−506282.3	5.72
4-HADNT	0.0199(56)	−0.3529(55)	0.3728	−506280.0	4.07
2-ADNT	0.0140(52)	−0.3437(51)	0.3577	−459340.7	6.02
4-ADNT	0.0189(52)	−0.3396(51)	0.3585	−459338.4	4.59

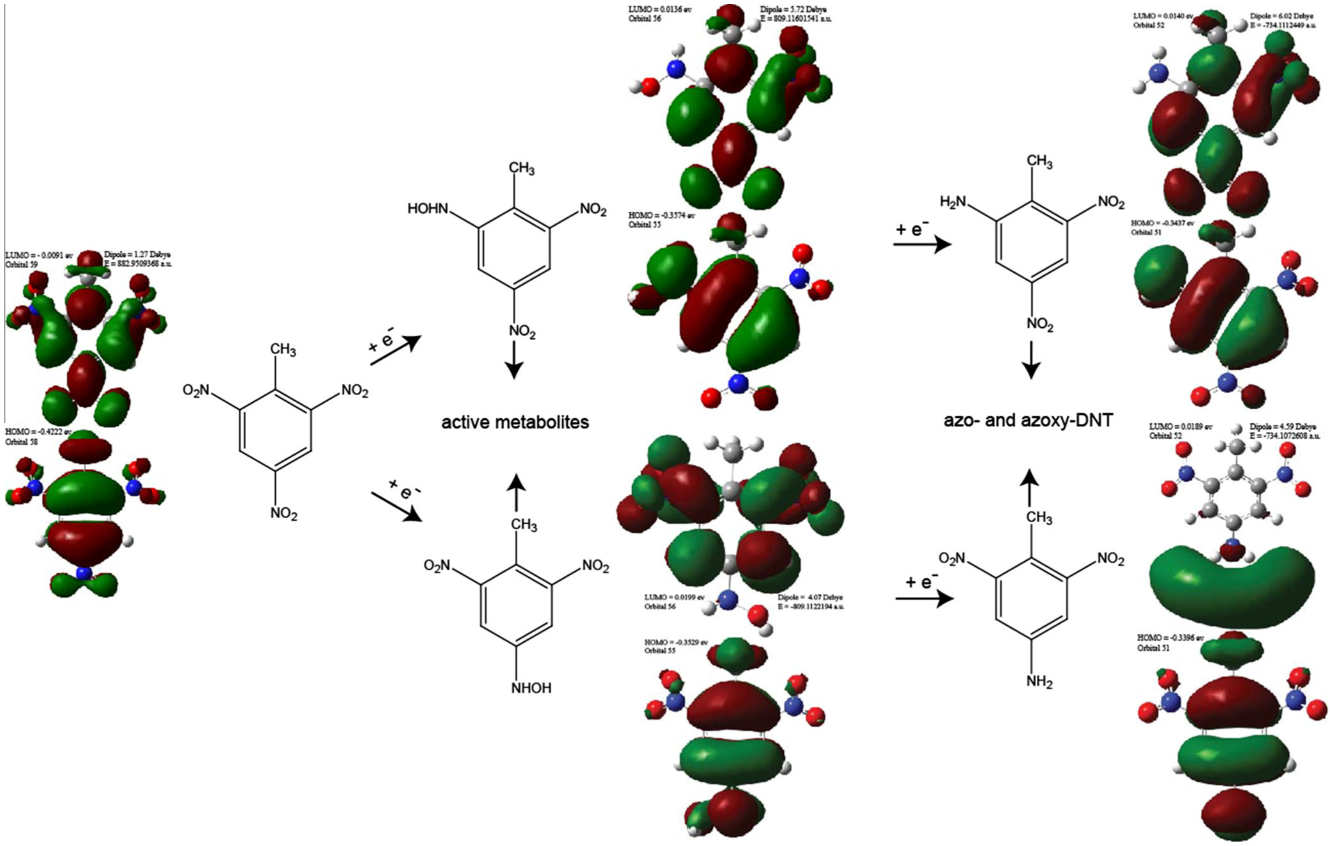

Fig. 6. Frontier orbital for TNT, 2-HADNT, 4-HADNT, 2-ADNT, and 4-ADNT, calculated using MP2/aug-cc-pVDZ.

Table 3
Chemical properties of 2-HADNT calculated using B3LYP and MP2 methods.

Method	LUMO (eV) (MO)	HOMO (eV) (MO)	LUMO–HOMO gap (eV)	Dipole (Debye)
B3LYP/6-311+G**	−0.1152(56)	−0.2704(55)	0.1552	6.56
B3LYP/aug-cc-pVDZ	−0.1119(56)	−0.2673(55)	0.1554	6.40
MP2/aug-cc-pVDZ	0.0136(56)	−0.3574(55)	0.3710	5.71

Table 4
Effect of inclusion of salvation model on the calculations of IR vibrational frequencies for 2-HADNT (cm^{-1}).

IR (solid)	B3LYP/6-311+G**	B3LYP/6-311+G** (DMSO)	B3LYP/aug-cc-pVDZ	B3LYP/aug-cc-pVDZ (DMSO)	Assignment
	844	837	830	837	2,4,6-C–N Scissors
1349	1353	1357	1364	1366	Symmetric stretching 4,6-NO_2
1536	1518	1515	1509	1505	Asymmetric stretching 4-NO_2
1638	1637	1633	1643	1639	Asymmetric stretching 6-NO_2

of 2-ADNT. Table 3 also shows that the LUMO–HOMO gaps of 2-HADNT and its isomer 4-HADNT are very close, which indicates the 2-HADNT and 4-HADNT have similar kinetic stability. In another word, mixture of the two isomers will not change their kinetic stability. From the results listed in Table 2, it was also found that the atomization energy of 2-HADNT and 2-ADNT are 2.3 kcal/mol lower than that of 4-HADNT and 4-ADNT, respectively, due to steric hindrance between 2-NO_2 and the methyl group. However the difference in the atomization energy can be reduced by replacing the 2-NO_2 group with −NHOH or NH_2. Dipole moment

Table 5
IR vibrational frequencies for 2-HADNT calculated from different method (cm^{-1}).

Raman (solid)	IR (solid)	B3LYP/6-311+G**	B3LYP/aug-cc-pVDZ	Mp2/aug-cc-pVDZ (DMSO)	Assignment
840	850	844	830	851	2,4,6-C–N Scissors
1350	1349	1353	1364	1380	Symmetric stretching 4,6-NO_2
	1536	1518	1509	1548	Asymmetric stretching 4-NO_2
1600	1638	1637	1643	1653	Asymmetric stretching 6-NO_2

Table 6
Comparison between experimental and calculated results for 2-HADNT and TNT (cm^{-1}).

TNT			2-HADNT			
Raman (solid)	IR (solid)	B3LYP/6-311+G**	Raman (solid)	IR (solid)	B3LYP/6-311+G**	Assignment
822	824	844	840	850	844	2,4,6-C–N Scissors
1359	1350	1370	1350	1349	1353	Symmetric stretching 4,6-NO_2
1534	1533	1590		1536	1518	Asymmetric stretching 4-NO_2
1602	1602	1646	1600	1638	1637	Asymmetric stretching 6-NO_2

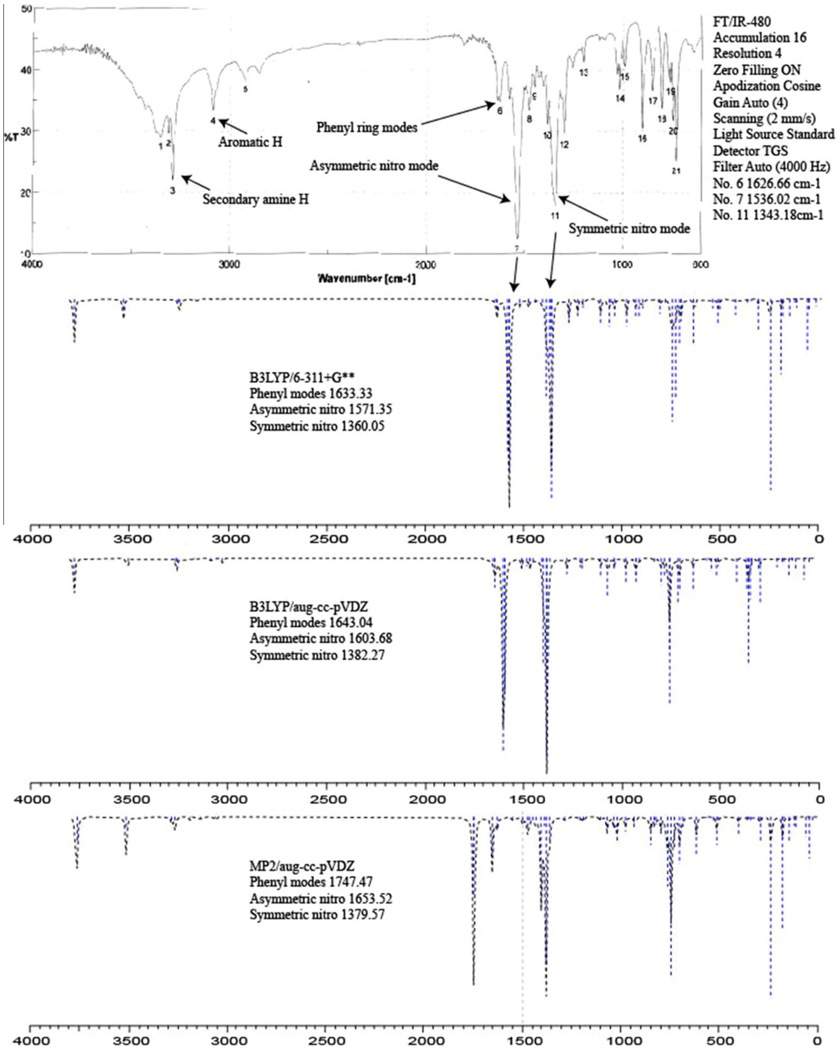

Fig. 7. Comparison of the experimental IR spectrum of 2-HADNT with calculated vibrational frequencies using B3LYP/6-311+G**, B3LYP/aug-cc-pVDZ, and MP2/aug-cc-pVDZ.

of 2-HADNT (5.72 Debye) and 2-ADNT (6.02 Debye) are much higher than that of TNT (1.27 Debye), and are also higher than their isomers 4-HADNT (4.07 Debye) and 4-ADNT (4.59 Debye).

The variability of LUMO–HOMO separations and dipole moments obtained from different chemistry models are listed in Table 3. The dipole moments 6.56 and 6.40 Debye calculated for 2-HADNT using B3LYP/6-311+G** and B3LYP/aug-cc-pVDZ, respectively, are only slightly higher than the 5.71 Debye obtained with MP2/aug-cc-pVDZ. In contrast, LUMO–HOMO separations of about 0.155 eV calculated from B3LYP evidently deviates from 0.3710 eV, which was obtained using MP2/au-cc-pVDZ. This apparent difference shows that appropriate chemistry model has to be carefully chosen for simulating frontier orbital of the TNT derivatives.

Vibrational frequency analysis

Vibrational frequencies were calculated for 2-HADNT based on the optimized structures obtained using B3LYP/6-311+G**, B3LYP/aug-cc-pVDZ, and MP2/aug-cc-pVDZ, and coupled with the SMD solvation model. Table 4 displays an example of calculated symmetric and asymmetric nitro vibrational frequencies using B3LYP coupled with SMD salvation model. All major symmetric and asymmetric C–N stretching absorptions calculated using B3LYP/6-311+G**, B3LYP/aug-cc-pVDZ, and MP2/aug-cc-pVDZ are listed in Table 5. TNT FTIR data [20] are included in Table 6 for comparison. IR and Raman absorption frequencies and intensities are related to the unique conformations and electronic states of the molecules. The roles of IR and Raman spectra in characterizations of compounds are almost complementary for centrosymmetrical molecules. For centrosymmetrical molecules, the IR and Raman absorptions can be both weak, both strong, and one weak and one strong at different wavelengths, but such characteristic is not that clear in asymmetric molecules such as 2-HADNT. Fig. 7 compares our experimental IR spectrum of 2-HADNT with calculated IR absorptions and a reasonable agreement was observed between the experimental and calculated absorptions using the B3LYP/6-311+G** method in spite of the differences between 2-HADNT molecules of the packed solid observed from experiments and 2-HADNT conformations of gas phase calculated from simulations. As can be seen from that figure, according to experimental observation, the strong asymmetric nitro model absorption occurred at 1536 cm^{-1}, which is very close to 1571.35 cm^{-1} as calculated using B3LYP/6-311+G** method. In contrast, B3LYP/aug-cc-pVDZ and MP2/aug-cc-pVDZ provided poor results (1603.58 cm^{-1} and 1653.52 cm^{-1} respectively). As demonstrated in previous studies, MP2 had difficulty in accurately predicting vibrational modes for aniline and phenol [47], even with extended basis sets [48]. According to Zierkiewicz and Michalska [49], Wojciechowski and Michalska [50], the good results obtained from B3LYP/++G** are somewhat surprising. The strongest IR and Raman absorptions for 2-HADNT in our study were observed at 1349 and 1350 cm^{-1}, respectively, for the symmetric stretching mode of the 4,6 C–N bonds. However, these absorptions were identified at 1600 and 1638 cm^{-1}, respectively, for asymmetric stretching mode of the 4,6 nitro groups. These absorptions can be used in the qualitative analysis and onsite monitoring of 2-HADNT in TNT contaminated environment.

Conclusion

In this study, chemical properties of TNT metabolite 2-HADNT were determined through both mechanical simulations and experimental measurements and structural optimization was carried out. The LUMO–HOMO gaps were fist calculated for TNT and its degradation products and used to evaluate their kinetic stabilities. p-π interactions between 4-nitro and phenyl ring were analyzed to clarify the conformational distributions of TNT and its degradation products.

In this study, the minimum energy conformations calculated from the quantum mechanical analysis are very close to those observed from the crystallography. Such a good agreement was further verified through potential energy scans along the coordinates corresponding to the rotations of the four functional groups. The most remarkable observation is that the 4-nitro group exhibits nearly co-planarity with the phenyl ring in all crystal and optimized structures, in contrast to those in conformers of the TNT crystal structure. The electron donating nature of the 2-hydroxylamino group imposes only limited effects on the co-planarity and the aromatic conjugation. On inspecting the LUMO energy, HOMO energy, and LUMO–HOMO energy separation calculated from MP2 and B3LYP methods, considerable discrepancies were found. Therefore, in applying DFT methods for simulations, the chemistry model has to be carefully selected and even needs to be verified through *ab initio* MP2 methods in order to achieve a qualitative model and obtain accurate results.

In summary, important findings of this research include that: (1) the kinetic stability of 2-HADNT is lower than that of TNT; (2) un-conjugated conformation is thermally accessible due to the lower energy barrier for both TNT and 2-HADNT; and (3) the popular DFT method should be chosen with cautions because significant discrepancy between the DFT results and MP2 results was identified. The results found from this study can help researchers to better understand the compound of 2-HADNT and to develop effective management plans to prevent its leakage so as to minimize its impact on the environment.

References

[1] T.B. Brill, K.J. James, J. Phys. Chem. 97 (34) (1993) 8759–8763.
[2] J.C. Oxley, J.L. Smith, H. Ye, R.L. McKenney, P.R. Bolduc, J. Phys. Chem. 99 (23) (1995) 9593–9602.
[3] R.M. Vrcelj, H.G. Gallagher, J.N. Sherwood, J. Am. Chem. Soc. 123 (10) (2001) 2291–2295.
[4] D.R. Ownby, J.B. Belden, G.R. Lotufo, M.J. Lydy, Chemosphere 58 (9) (2005) 1153–1159.
[5] J.B. Belden, D.R. Ownby, G.R. Lotufo, M.J. Lydy, Chemosphere 58 (9) (2005) 1161–1168.
[6] G. Adamia, M. Ghoghoberidze, D. Graves, G. Khatisashvili, G. Kvesitadze, E. Lomidze, D. Ugrekhelidze, G. Zaalishvili, Ecotoxicol. Environ. Saf. 64 (2) (2006) 136–145.
[7] A.M. Ziganshin, R.P. Naumova, A.J. Pannier, R. Gerlach, Chemosphere 79 (4) (2010) 426–433.
[8] R. Bajpai, D. Parekh, S. Herrmann, M. Popovic, J. Paca, M. Qasim, J. Hazard. Mater. 106 (1) (2004) 55–66.
[9] Z. Li, P. Shea, S. Comfort, J. Environ. Qual. 26 (1997) 480–487.
[10] M. Qasim, L. Gorb, D. Magers, P. Honea, J. Leszczynski, B. Moore, L. Taylor, M. Middleton, J. Hazard. Mater. 167 (1–3) (2009) 154–163.
[11] T. Junk, W.J. Catallo, Chem. Spec. Bioavailab. 10 (2) (1998) 47–52.
[12] J. Michels, G. Gottschalk, Appl. Environ. Microbiol. 60 (1) (1994) 187–194.
[13] T. Maeda, N. Nagafuchi, A. Kubota, K. Kadokami, H.I. Ogawa, J. Chromatogr. Sci. 44 (2) (2006) 96–100.
[14] S. Homma-Takeda, Y. Hiraku, Y. Ohkuma, S. Oikawa, M. Murata, K. Ogawa, T. Iwamuro, S. Li, G.-F. Sun, Y. Kumagai, N. Shimojo, S. Kawanishi, Free Radical Res. 36 (5) (2002) 555–566.
[15] P.J. Groenewegen, J.M. Bont, Arch. Microbiol. 158 (5) (1992) 381–386.
[16] M. Qasim, Y. Kholod, L. Gorb, D. Magers, P. Honea, J. Leszczynski, Chemosphere 69 (7) (2007) 1144–1150.
[17] W.R. Carper, L.P. Davis, M.W. Extine, J. Phys. Chem. 86 (4) (1982) 459–462.
[18] N.I. Golovina, A.N. Titkov, A.V. Raevskii, L.O. Atovmyan, J. Solid State Chem. 113 (2) (1994) 229–238.
[19] J.C. Barnes, W. Golnazarians, Acta Crystallogr. C 43 (3) (1987) 549–552.
[20] F. Gerard, A. Hardy, Acta Crystallogr. C 44 (7) (1988) 1283–1287.
[21] S. Neyertz, D. Mathieu, S. Khanniche, D. Brown, J. Phys. Chem. A 116 (32) (2012) 8374–8381.
[22] R. Infante-Castillo, S.P. Hernandez-Rivera, Adv. Phys. Chem. 2012 (2012) 1–11.
[23] J. Quenneville, M. Greenfield, D.S. Moore, S.D. McGrane, R.J. Scharff, J. Phys. Chem. A 115 (44) (2011) 12286–12297.
[24] J.B. Cabalo, R. Sausa, J. Phys. Chem. A 115 (33) (2011) 9139–9150.
[25] R. Cohen, Y. Zeiri, E. Wurzberg, R. Kosloff, J. Phys. Chem. A 111 (43) (2007) 11074–11083.
[26] W.A. Al-Saidi, S.A. Asher, P. Norman, J. Phys. Chem. A 116 (30) (2012) 7862–7872.
[27] X.-F. Chen, C.-Y. Hou, K.-L. Han, J. Phys. Chem. A 114 (2) (2009) 1169–1177.
[28] A. Michalkova, L. Gorb, F. Hill, J. Phys. Chem. A 115 (11) (2011) 2423–2430.
[29] S.P. Hernández-Rivera, J. Castillo-Chará, Vib. Spectrosc. 53 (2) (2010) 248–259.
[30] J. Clarkson, W.E. Smith, D.N. Batchelder, D.A. Smith, A.M. Coats, J. Mol. Struct. 648 (3) (2003) 203–214.
[31] L.F. Alzate, C.M. Ramos, N.M. Hernandez, S.P. Hernandez, N. Mina, Vib. Spectrosc. 42 (2) (2006) 357–368.
[32] P.J. Stephens, F.J. Devlin, C.F. Chabalowski, M.J. Frisch, J. Phys. Chem. 98 (45) (1994) 11623–11627.
[33] A. Becke, J. Chem. Phys. 98 (7) (1993) 5648.
[34] C. Lee, W. Yang, R.G. Parr, Phys. Rev. B 37 (2) (1988) 785.
[35] S.H. Vosko, L. Wilk, M. Nusair, Can. J. Phys. 58 (8) (1980) 1200–1211.

[36] M.D. Wodrich, C. Corminboeuf, P.V.R. Schleyer, Org. Lett. 8 (17) (2006) 3631–3634.

[37] R.I. Zubatyuk, L. Gorb, O.V. Shishkin, M. Qasim, J. Leszczynski, J. Comput. Chem. 31 (1) (2010) 144–150.

[38] M.J. Frisch, G.W. Trucks, H.B. Schlegel, G.E. Scuseria, Gaussian 09 Revision A.1, Gaussian, Inc.: Wallingford, CT, USA, 2009.

[39] J.V. Burda, A. Toro-Labbe, S. Gutierrez-Oliva, J.S. Murray, P. Politzer, J. Phys. Chem. A 111 (13) (2007) 2455–2457.

[40] U. Bren, M. Zupan, F.P. Guengerich, J. Mavri, J. Org. Chem. 71 (11) (2006) 4078–4084.

[41] A.V. Marenich, C.J. Cramer, D.G. Truhlar, J. Phys. Chem. B 113 (18) (2009) 6378–6396.

[42] M.K. Gilson, B.H. Honig, Biopolymers 25 (11) (2004) 2097–2119.

[43] K. Fukui, T. Yonezawa, C. Nagata, J. Chem. Phys. 27 (6) (1957) 1247–1259.

[44] J.-I. Aihara, J. Phys. Chem. A 103 (37) (1999) 7487–7495.

[45] X. Liu, T.G. Schmalz, D.J. Klein, Chem. Phys. Lett. 188 (5–6) (1992) 550–554.

[46] W. Zou, W. Liu, L. Luo, S. Zhang, R. Lu, G. Veser, J. Mater. Chem. 22 (25) (2012) 12474–12478.

[47] P. Wojciechowski, K. Helios, D. Michalska, Vib. Spectrosc. 57 (1) (2011) 126–134.

[48] D. Michalska, W. Zierkiewicz, D.C. Bienko, W. Wojciechowski, T. Zeegers-Huyskens, J. Phys. Chem. A 105 (38) (2001) 8734–8739.

[49] W. Zierkiewicz, D. Michalska, J. Phys. Chem. A 107 (22) (2003) 4547–4554.

[50] P.M. Wojciechowski, D. Michalska, Spectrochim. Acta Part A Mol. Biomol. Spectrosc. 68 (3) (2007) 948–955.